Equivalent Circuit for Electromagnetic Interaction and Transmission Through Graphene Sheets

Giampiero Lovat, *Member, IEEE*

***Abstract*—An equivalent circuit for the analysis of the interaction between an electromagnetic field and a thin graphene sheet is derived, based on a local anisotropic model of the graphene conductivity, valid at frequencies below the THz range. Due to the anisotropic properties, the equivalent circuit is a four-port network which couples the fundamental TE and TM polarizations. The possible effects of electrostatic and/or magnetostatic bias are included and the equivalent circuit is next used to investigate the shielding properties of graphene layers against impinging plane waves. While the possibility of tuning the graphene conductivity leads to interesting properties of electronic control of shielding perfomance, the proposed equivalent circuit represents a very simple tool for the relevant analysis and design.**

***Index Terms*—Electromagnetic shielding, equivalent circuits, graphene, nanotechnology.**

I. Introduction

GRAPHENE is the 2-D version of graphite and is one of the most promising materials in future micro- and nanotechnology due to its excellent mechanical properties and the capability to sustain extremely large electric currents (more than 10^8 A/cm^2). Basically, graphene consists of an atomically thick layer of carbon atoms arranged in a honeycomb structure and can be viewed as the building block of other graphitic carbon allotropes; fullerenes can be seen to be made by wrapping a section of graphene sheet; carbon nanotubes can be made by rolling graphene sheets in a cylinder; and graphite is made of graphene sheets stacked on top of each other [1]. Only recently single layers of graphite have been isolated, using micromechanical cleavage; since then, this subject has gained the attention of many research groups all over the world and the advent of mass production technologies for graphene is allowing the development of unimaginable applications in many fields [2].

From an electronic point of view, graphene is a zero bandgap semiconductor whose conductivity can be tuned by electrostatic and/or magnetostatic bias through the electric-field and Hall effects [3], [4]; however, with respect to other atomic thin metal films, graphene is thermodynamically stable and possesses a minimum conductivity also for a vanishing carrier concentration [5]. However, also graphene is affected by disorder, and its conductivity can strongly depend on the environment; in particular, extrinsic and intrinsic effects exist which can be sources of disorder [6].

From an electromagnetic point of view, graphene can be described as an infinitesimally thin medium characterized by a surface conductivity [7]; based on a microscopic quantum-dynamical approach, a mathematical model for such a conductivity has been derived which also includes the important effects of electrostatic and/or magnetostatic bias [8]. In the presence of both an electric and a magnetic bias, an *anistropic* conductivity has to be considered, which is therefore described by a *dyadic* quantity. Besides, as pointed out in [9], it should be noted that, starting from THz frequencies, spatial-dispersion effects may arise, which also require the use of an anisotropic model even in the absence of bias fields.

In this work, the equivalent circuit of a planar surface characterized by an anisotropic conductivity is first derived starting from Maxwell's equations and, next, the electromagnetic model of graphene is adopted in order to derive the equivalent circuit of graphene sheets to be used in the classical transmission-line analysis of the shielding behavior of planar screens [10] (in fact, nanostructured materials have recently attracted the attention of the EMC community [11]–[13]). The derived equivalent circuit can thus be used to evaluate the shielding properties of graphene sheets illuminated by uniform plane waves in a variety of configurations: unbiased graphene, electrostatically or magnetostatically biased graphene, and graphene sheets in multilayer configurations. In addition, the equivalent circuit can also be used for the analysis of the interaction between a finite source and the graphene sheets once combined with the classical transmission-line network formulation for the computation of dyadic Green's functions in stratified media [14]; the latter represents a useful alternative to the approach based on the electromagnetic potentials developed in [7] and [9].

The paper is organized as follows. In Section II the four-port equivalent circuit of a conductive sheet with anisotropic conductivity is derived and it is shown how the anisotropic behavior couples the fundamental TE and TM polarizations; in particular, for each polarization, the anisotropic conductive sheet is represented through a shunt admittance and a parallel voltage-controlled current generator. In Section III, the graphene conductivity is introduced and briefly discussed, while in Section IV the general equivalent circuit derived in Section II is adopted to model the graphene sheet in different operating conditions (unbiased and electrostatically and/or magnetostatically biased). In Section V, the equivalent circuit is used to study the shielding properties of graphene sheets and investigate the potential applications of this material as electromagnetic shield and cover. Finally, in Section VI conclusions are drawn.

Manuscript received April 29, 2011; revised July 20, 2011; accepted September 14, 2011. Date of publication October 13, 2011; date of current version February 17, 2012.

The author is with the Department of Astronautical, Electrical, and Energetic Engineering, "Sapienza" University of Rome, 00184 Rome, Italy (e-mail: giampiero.lovat@uniroma1.it).

Digital Object Identifier 10.1109/TEMC.2011.2169072

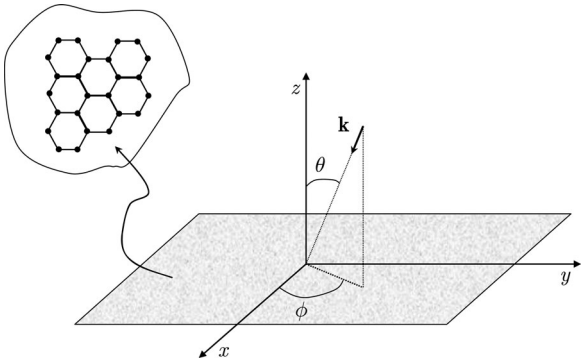

Fig. 1. Plane-wave incidence on a graphene sheet.

II. Equivalent Circuit of an Anisotropic Conductive Surface

Let us consider an infinitesimally thin conductive sheet with anisotropic conductivity $\underline{\underline{\boldsymbol{\sigma}}}$ separating two air regions and assume that the sheet is located over the $z = 0$ plane so that

$$\underline{\underline{\boldsymbol{\sigma}}} = \begin{bmatrix} \sigma_{xx} & \sigma_{xy} \\ \sigma_{yx} & \sigma_{yy} \end{bmatrix}. \tag{1}$$

As sketched in Fig. 1, a uniform plane wave impinges from the direction (θ, ϕ) in the half-space $z > 0$ with wavenumber $\mathbf{k} = \mathbf{u}_x k_x + \mathbf{u}_y k_y + \mathbf{u}_z k_z$, where $k_x = k_0 n_x$, $k_y = k_0 n_y$, $k_z = k_0 n_z$ with $n_x = -\cos\phi \sin\theta$, $n_y = -\sin\phi \sin\theta$, $n_z = -\cos\theta$, while $k_0 = 2\pi/\lambda_0$ is the free-space wavenumber. By using the classical analogy between uniform plane-wave propagation in stratified media and the propagation of voltage and current waves on a uniform transmission line, the relevant tangential electric and magnetic fields for the fundamental TE_z and TM_z polarizations can be expressed as [10], [14]

$$\begin{aligned} \mathbf{E}_\tau^{\mathrm{TE/TM}}(x,y,z) &= T(x,y) V^{\mathrm{TE/TM}}(z) \mathbf{e}^{\mathrm{TE/TM}} \\ \mathbf{H}_\tau^{\mathrm{TE/TM}}(x,y,z) &= T(x,y) I^{\mathrm{TE/TM}}(z) \mathbf{h}^{\mathrm{TE/TM}} \end{aligned} \tag{2}$$

where $T(x,y) = e^{-j(k_x x + k_y y)}$, while $V^{\mathrm{TE/TM}}(z)$ and $I^{\mathrm{TE/TM}}(z)$ are solutions of TE and TM transmission-line like equations with propagation constant k_z and characteristic admittances

$$Y_0^{\mathrm{TE}} = \frac{n_z}{\eta_0}, \qquad Y_0^{\mathrm{TM}} = \frac{1}{\eta_0 n_z} \tag{3}$$

respectively, where η_0 is the free-space intrinsic impedance. The modal vectors $\mathbf{e}^{\mathrm{TE/TM}}$ and $\mathbf{h}^{\mathrm{TE/TM}}$ are defined as

$$\begin{aligned} \mathbf{e}^{\mathrm{TE}} &= \frac{-n_y \mathbf{u}_x + n_x \mathbf{u}_y}{\sqrt{n_x^2 + n_y^2}} \\ \mathbf{h}^{\mathrm{TE}} &= \frac{-n_x \mathbf{u}_x - n_y \mathbf{u}_y}{\sqrt{n_x^2 + n_y^2}} \end{aligned} \tag{4}$$

and

$$\begin{aligned} \mathbf{e}^{\mathrm{TM}} &= -n_z \frac{n_x \mathbf{u}_x + n_y \mathbf{u}_y}{\sqrt{n_x^2 + n_y^2}} \\ \mathbf{h}^{\mathrm{TM}} &= n_z \frac{n_y \mathbf{u}_x - n_x \mathbf{u}_y}{\sqrt{n_x^2 + n_y^2}}. \end{aligned} \tag{5}$$

The longitudinal components of the TE magnetic field and TM electric field are related to the above-mentioned voltages and currents through [14]

$$\begin{aligned} H_z^{\mathrm{TE}}(\mathbf{r}) &= \frac{\sqrt{n_x^2 + n_y^2}}{\eta_0} T(x,y) V^{\mathrm{TE}}(z) \\ E_z^{\mathrm{TM}}(\mathbf{r}) &= \eta_0 n_z \sqrt{n_x^2 + n_y^2}\, T(x,y) I^{\mathrm{TM}}(z). \end{aligned} \tag{6}$$

The most general plane wave can be written as the sum of a TE and a TM (with respect to z) plane wave, i.e., for the tangential fields

$$\begin{aligned} \mathbf{E}_\tau(\mathbf{r}) &= A^{\mathrm{TE}} \mathbf{E}_\tau^{\mathrm{TE}}(\mathbf{r}) + A^{\mathrm{TM}} \mathbf{E}_\tau^{\mathrm{TM}}(\mathbf{r}) \\ \mathbf{H}_\tau(\mathbf{r}) &= B^{\mathrm{TE}} \mathbf{H}_\tau^{\mathrm{TE}}(\mathbf{r}) + B^{\mathrm{TM}} \mathbf{H}_\tau^{\mathrm{TM}}(\mathbf{r}) \end{aligned} \tag{7}$$

where $A^{\mathrm{TE/TM}}$ and $B^{\mathrm{TE/TM}}$ are suitable coefficients.

In order to derive the equivalent circuit of the anisotropic conductive sheet, the boundary conditions at the sheet must be enforced, i.e.,

$$\mathbf{u}_z \times \left[\mathbf{E}_\tau(x,y,0^+)\right] = \mathbf{u}_z \times \left[\mathbf{E}_\tau(x,y,0^-)\right] \tag{8}$$

which implies

$$\mathbf{E}_\tau(x,y,0^+) = \mathbf{E}_\tau(x,y,0^-) = \mathbf{E}_\tau(x,y,0) \tag{9}$$

and

$$\mathbf{u}_z \times \left[\mathbf{H}_\tau(x,y,0^+) - \mathbf{H}_\tau(x,y,0^-)\right] = \underline{\underline{\boldsymbol{\sigma}}} \cdot \mathbf{E}_\tau(x,y,0) \tag{10}$$

which, in turn, entails

$$\begin{aligned} H_y(x,y,0^-) - H_y(x,y,0^+) &= \sigma_{xx} E_x(x,y,0) + \sigma_{xy} E_y(x,y,0) \\ H_x(x,y,0^+) - H_x(x,y,0^-) &= \sigma_{yx} E_x(x,y,0) + \sigma_{yy} E_y(x,y,0). \end{aligned} \tag{11}$$

By expressing all the transverse components in (9) and (11) in terms of the TE and TM voltages and currents we obtain

$$\begin{aligned} V^{\mathrm{TE}}(0^+) &= V^{\mathrm{TE}}(0^-) = V^{\mathrm{TE}}(0) \\ V^{\mathrm{TM}}(0^+) &= V^{\mathrm{TM}}(0^-) = V^{\mathrm{TM}}(0) \end{aligned} \tag{12}$$

and

$$\begin{aligned} &- n_y I^{\mathrm{TE}}(0^+) - n_x I^{\mathrm{TM}}(0^+) + n_y I^{\mathrm{TE}}(0^-) + n_x I^{\mathrm{TM}}(0^-) \\ &\quad = -\sigma_{xx} \left[-n_y V^{\mathrm{TE}}(0) - n_x V^{\mathrm{TM}}(0)\right] \\ &\qquad - \sigma_{xy} \left[n_x V^{\mathrm{TE}}(0) - n_y V^{\mathrm{TM}}(0)\right] \\ &- n_x I^{\mathrm{TE}}(0^+) + n_y I^{\mathrm{TM}}(0^+) + n_x I^{\mathrm{TE}}(0^-) - n_y I^{\mathrm{TM}}(0^-) \\ &\quad = \sigma_{yx} \left[-n_y V^{\mathrm{TE}}(0) - n_x V^{\mathrm{TM}}(0)\right] \\ &\qquad + \sigma_{yy} \left[n_x V^{\mathrm{TE}}(0) - n_y V^{\mathrm{TM}}(0)\right]. \end{aligned} \tag{13}$$

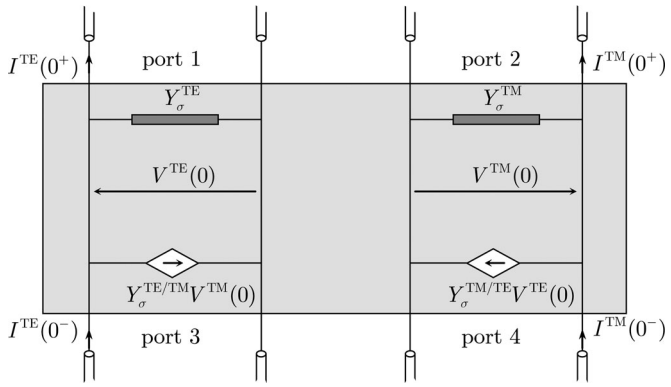

Fig. 2. Equivalent circuit of an anisotropic conductive sheet.

By solving the linear system in (13) in terms of the unknowns $I^{\mathrm{TE}}(0^-)$ and $I^{\mathrm{TM}}(0^-)$, we have

$$\begin{aligned} I^{\mathrm{TE}}(0^-) &= I^{\mathrm{TE}}(0^+) + Y_\sigma^{\mathrm{TE}} V^{\mathrm{TE}}(0) + Y_\sigma^{\mathrm{TE/TM}} V^{\mathrm{TM}}(0) \\ I^{\mathrm{TM}}(0^-) &= I^{\mathrm{TM}}(0^+) + Y_\sigma^{\mathrm{TM}} V^{\mathrm{TM}}(0) + Y_\sigma^{\mathrm{TM/TE}} V^{\mathrm{TE}}(0) \end{aligned} \tag{14}$$

where

$$\begin{aligned} Y_\sigma^{\mathrm{TE}} &= \frac{n_y^2\sigma_{xx} + n_x^2\sigma_{yy} - n_x n_y\left(\sigma_{xy} + \sigma_{yx}\right)}{n_x^2 + n_y^2} \\ Y_\sigma^{\mathrm{TM}} &= \frac{n_x^2\sigma_{xx} + n_y^2\sigma_{yy} + n_x n_y\left(\sigma_{xy} + \sigma_{yx}\right)}{n_x^2 + n_y^2} \end{aligned} \tag{15}$$

and

$$\begin{aligned} Y_\sigma^{\mathrm{TE/TM}} &= \frac{n_y^2\sigma_{xy} - n_x^2\sigma_{yx} + n_x n_y\left(\sigma_{xx} - \sigma_{yy}\right)}{n_x^2 + n_y^2} \\ Y_\sigma^{\mathrm{TM/TE}} &= \frac{n_y^2\sigma_{yx} - n_x^2\sigma_{xy} + n_x n_y\left(\sigma_{xx} - \sigma_{yy}\right)}{n_x^2 + n_y^2}. \end{aligned} \tag{16}$$

From (14), the sought equivalent circuit of the anisotropic conductive sheet can be deduced; in fact, it is easy to verify that (14) represents the constitutive relations of a four-port network: two ports (ports 1 and 3) represent the input and output TE waves, respectively, while the other two ports (ports 2 and 4) represent the input and output TM waves, respectively. The input and output are related through a shunt susceptance and a voltage-controlled current generator, which also represents the coupling term between the two fundamental polarizations. The relevant equivalent circuit is reported in Fig. 2.

The derived equivalent circuit will next be used to model biased and possibly anisotropic graphene sheets.

III. Electromagnetic Model of Graphene

As mentioned in the Introduction, a graphene sheet can be modeled as a conductive sheet with a possibly anisotropic conductivity. The anisotropic characteristic may arise from two different mechanisms: i) presence of a magnetostatic bias or ii) spatial-dispersion effects [9]; however, the latter can usually be neglected below the THz regime and will not be addressed here. Therefore, in general, in the microwave regime or below, the conductivity of graphene has an expression as in (1), where the dyadic elements depend on different parameters, e.g., frequency $f = \omega/(2\pi)$, temperature T, and a phenomenological scattering rate Γ [8]; moreover, in the presence of a bias field, they also depend on the applied electrostatic bias $\mathbf{E}_{\mathrm{bias}} = \mathbf{u}_z E_{\mathrm{bias}}$ or the applied magnetostatic bias $\mathbf{B}_{\mathrm{bias}} = \mathbf{u}_z B_{\mathrm{bias}}$. The mathematical expressions for the dyadic elements have been derived in [8] starting from the Kubo formula [15]. In particular, with reference to (1), it results

$$\begin{aligned} \sigma_{xx} &= \sigma_{yy} = \sigma_{\mathrm{D}} \\ \sigma_{xy} &= -\sigma_{yx} = \sigma_{\mathrm{O}} \end{aligned} \tag{17}$$

with

$$\begin{aligned} \sigma_{\mathrm{D}} = \sigma_{\mathrm{DR}} - j\sigma_{\mathrm{DJ}} &= j\frac{q_e^2 v_{\mathrm{F}}^2 \left| q_e B_{\mathrm{bias}} \right| \left(\omega - j2\Gamma\right)\hbar}{\pi} \\ &\cdot \sum_{n=0}^{\infty} \left\{ \frac{n_{\mathrm{F}}\left(M_n\right) - n_{\mathrm{F}}\left(M_{n+1}\right) + n_{\mathrm{F}}\left(-M_{n+1}\right) - n_{\mathrm{F}}\left(-M_n\right)}{\left(M_{n+1} - M_n\right)^2 - \left(\omega - j2\Gamma\right)^2\hbar^2} \right. \\ &\cdot \left(1 - \frac{\Delta^2}{M_n M_{n+1}}\right) \frac{1}{M_{n+1} - M_n} \\ &+ \frac{n_{\mathrm{F}}\left(-M_n\right) - n_{\mathrm{F}}\left(M_{n+1}\right) + n_{\mathrm{F}}\left(-M_{n+1}\right) - n_{\mathrm{F}}\left(M_n\right)}{\left(M_{n+1} + M_n\right)^2 - \left(\omega - j2\Gamma\right)^2\hbar^2} \\ &\left. \cdot \left(1 + \frac{\Delta^2}{M_n M_{n+1}}\right) \frac{1}{M_{n+1} + M_n} \right\} \end{aligned} \tag{18}$$

and

$$\begin{aligned} \sigma_{\mathrm{O}} = \sigma_{\mathrm{OR}} - j\sigma_{\mathrm{OJ}} &= -\frac{q_e^3 v_{\mathrm{F}}^2 B_{\mathrm{bias}}}{\pi} \\ &\cdot \sum_{n=0}^{\infty} \left[n_{\mathrm{F}}\left(M_n\right) - n_{\mathrm{F}}\left(M_{n+1}\right) + n_{\mathrm{F}}\left(-M_{n+1}\right) - n_{\mathrm{F}}\left(-M_n\right) \right] \\ &\cdot \left\{ \left(1 - \frac{\Delta^2}{M_n M_{n+1}}\right) \frac{1}{\left(M_{n+1} - M_n\right)^2 - \left(\omega - j2\Gamma\right)^2\hbar^2} \right. \\ &\left. + \left(1 + \frac{\Delta^2}{M_n M_{n+1}}\right) \frac{1}{\left(M_{n+1} + M_n\right)^2 - \left(\omega - j2\Gamma\right)^2\hbar^2} \right\} \end{aligned} \tag{19}$$

where

$$M_n = \sqrt{\Delta^2 + 2n v_{\mathrm{F}}^2 \left| q_e B_{\mathrm{bias}} \right| \hbar}. \tag{20}$$

It can be shown that (17)–(19) satisfy the Kramers–Krönig relationships [8]. As previously mentioned, if $B_{\mathrm{bias}} = 0$ or $E_{\mathrm{bias}} = 0$, it also results $\sigma_{\mathrm{O}} = 0$ and the graphene is characterized by an *isotropic* conductivity $\sigma = \sigma_{\mathrm{D}}$ (in fact, σ_{O} is an odd function of both B_{bias} and E_{bias}).

Several symbols and parameters are introduced in (18) and (19), which are explained here. First of all, $-q_e$ is the electron charge, $v_F \simeq 10^6$ m/s is the Fermi velocity in graphene, $\hbar$ is the reduced Planck's constant, and Δ is an excitonic energy gap with no effects at room temperature (so it will be assumed $\Delta = 0$ in what follows). Finally, n_{F} is the Fermi–Dirac

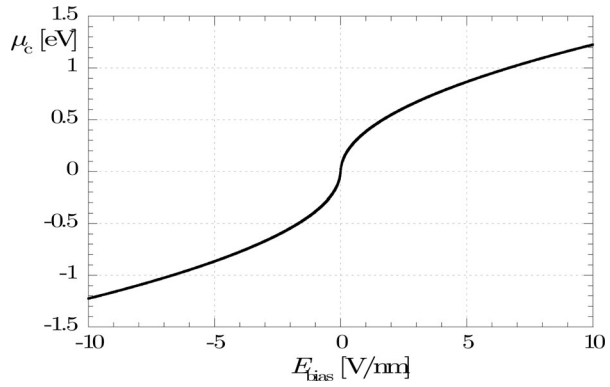

Fig. 3. Graphical representation of the relation between the chemical potential $\mu_{\rm c}\,(E_{\rm bias})$ and the electrostatic bias field $E_{\rm bias}$.

distribution given by

$$n_{\rm F}(\epsilon) = \frac{1}{1+e^{(\epsilon-\mu_{\rm c})/(k_{\rm B}T)}} \tag{21}$$

where ϵ is the energy, $k_{\rm B}$ is the Boltzmann's constant, and $\mu_{\rm c}$ is the chemical potential depending on the applied electrostatic bias $E_{\rm bias}$, which can easily be tuned from -1 eV to $+1$ eV with typical values of the bias fields (of the order of few V/nm); in particular, the relation between the chemical potential $\mu_{\rm c}$ and the electrostatic bias field $E_{\rm bias}$ is given by [9]

$$\frac{\varepsilon_0\pi\hbar^2 v_F^2}{q_{\rm e}}\,E_{\rm bias} = \int_0^{+\infty} \epsilon\left[n_{\rm F}(\epsilon) - n_{\rm F}(\epsilon+2\mu_{\rm c})\right]{\rm d}\epsilon \tag{22}$$

which must be solved numerically for the chemical potential $\mu_{\rm c}\,(E_{\rm bias})$; such a relation is represented graphically in Fig. 3. Alternatively, $\mu_{\rm c}$ can also be controlled by chemical doping. It should be noted that, if $\mu_{\rm c}=0$ (e.g., in the absence of electric bias and chemical doping), $\sigma_{\rm O}=0$ and the graphene presents an isotropic behavior with $\sigma=\sigma_{\rm D}$.

It can be shown that in the limit of small values of $B_{\rm bias}$, (18) and (19) reduce to

$$\begin{aligned}\sigma_{\rm D} &= j\frac{q_e^2\,(\omega-j2\Gamma)}{\pi\hbar}\\ &\cdot\left\{\frac{1}{(\omega-j2\Gamma)^2}\int_\Delta^{+\infty}\frac{\epsilon^2-\Delta^2}{\epsilon}\left[\frac{\partial n_F(\epsilon)}{\partial\epsilon}-\frac{\partial n_F(-\epsilon)}{\partial\epsilon}\right]{\rm d}\epsilon\right.\\ &\left.-\int_\Delta^{+\infty}\frac{\epsilon^2+\Delta^2}{\epsilon^2}\,\frac{n_F(\epsilon)-n_F(-\epsilon)}{(\omega-j2\Gamma)^2-4\,(\epsilon/\hbar)^2}\,{\rm d}\epsilon\right\}\end{aligned} \tag{23}$$

and

$$\begin{aligned}\sigma_{\rm O} &= -\frac{q_e^3 v_{\rm F}^2 B_{\rm bias}}{\pi\hbar^2}\int_\Delta^{+\infty}\left[\frac{\partial n_{\rm F}(\epsilon)}{\partial\epsilon}+\frac{\partial n_{\rm F}(-\epsilon)}{\partial\epsilon}\right]\\ &\cdot\left[\frac{\epsilon^2-\Delta^2}{\epsilon^2}\frac{1}{(\omega-j2\Gamma)^2}+\frac{\epsilon^2+\Delta^2}{\epsilon^2}\frac{1}{(\omega-j2\Gamma)^2-4\,(\epsilon/\hbar)^2}\right]{\rm d}\epsilon\end{aligned} \tag{24}$$

respectively, which can easily be computed through standard adaptive integration routines.

Finally, for $\Delta=0$, (23) can be approximately evaluated in a closed form as

$$\sigma_{\rm D} \simeq -j\frac{q_e^2 k_{\rm B}T}{\pi\hbar^2\,(\omega-j2\Gamma)}\left[\frac{\mu_{\rm c}}{k_{\rm B}T}+2\ln\left(1+e^{-\frac{\mu_{\rm c}}{k_{\rm B}T}}\right)\right] \tag{25}$$

thus showing a Drude-like behavior. Equation (25) is very accurate at room temperatures and below the THz regime.

IV. Equivalent Circuit of Graphene Sheets

The graphene conductivity tensor described in Section III can now be used in the equivalent circuit derived in Section II to obtain the equivalent circuit of a graphene sheet. The graphene sheet is assumed to be of infinite extent; this is obviously a crude approximation, since the lateral dimensions are today smaller than 1 mm, but the fabrication processes are rapidly improving; however, the approximation is accurate provided that electronic-edge and electromagnetic edge-diffraction effects can be neglected.

By substituting (17) in (15) and (16), the latter are greatly simplified, and it simply results

$$\begin{aligned}Y_\sigma^{\rm TE} &= Y_\sigma^{\rm TM} = \sigma_{\rm D}\\ Y_\sigma^{\rm TE/TM} &= -Y_\sigma^{\rm TM/TE} = \sigma_{\rm O}.\end{aligned} \tag{26}$$

Moreover, by separately studying the TE and TM plane-wave incidence problem, the equivalent circuit in Fig. 2 is also dramatically simplified leading to very simple expressions for the reflection and transmission coefficients. This is addressed in the sections to follow.

A. TE Plane-Wave Incidence

Let us consider the problem depicted in Fig. 1, where a plane wave impinges on a graphene sheet; let us assume that the incident plane wave is TE polarized. We are interested in applying the equivalent circuit in Fig. 2 to determine the electric and magnetic field in both the half-spaces $z>0$ and $z<0$. To this end, based on (2) and (6), it is sufficient to determine the voltages $V^{\rm TE/TM}(0)$ and the currents $I^{\rm TE/TM}\,(0^+)$ and $I^{\rm TE/TM}\,(0^-)$. In fact, for instance, for the electric field in $z<0$ it results

$$\begin{aligned}\mathbf{E}(\mathbf{r}) &= T(x,y)e^{jk_z z}big[\mathbf{e}^{\rm TE}V^{\rm TE}(0)\\ &+\mathbf{e}^{\rm TM}V^{\rm TM}(0)+n_z\sqrt{n_x^2+n_y^2}\eta_0 I^{\rm TM}(0^-)\mathbf{u}_z\big].\end{aligned} \tag{27}$$

If the incident plane wave is TE polarized, we have an incident voltage $V^{\rm inc}(z)=V_0^{\rm inc}e^{jk_z z}$ at port 1 in the equivalent circuit of Fig. 2, while all the other ports are closed on the relevant characteristic admittances $Y_0^{\rm TE}$ and $Y_0^{\rm TM}$, as reported in Fig. 4(a). Taking into account that it simply results

$$V^{\rm TM}(0) = -\frac{Y_\sigma^{\rm TM/TE}}{2Y_0^{\rm TM}+Y_\sigma^{\rm TM}}V^{\rm TE}(0) = \frac{\sigma_{\rm O}}{2Y_0^{\rm TM}+\sigma_{\rm D}}V^{\rm TE}(0) \tag{28}$$

the circuit is transformed in that reported in Fig. 4(b), where

$$Y_{\rm C}^{\rm TE} = -\frac{Y_\sigma^{\rm TE/TM}Y_\sigma^{\rm TM/TE}}{2Y_0^{\rm TM}+Y_\sigma^{\rm TM}} = \frac{\sigma_{\rm O}^2}{2Y_0^{\rm TM}+\sigma_{\rm D}}. \tag{29}$$

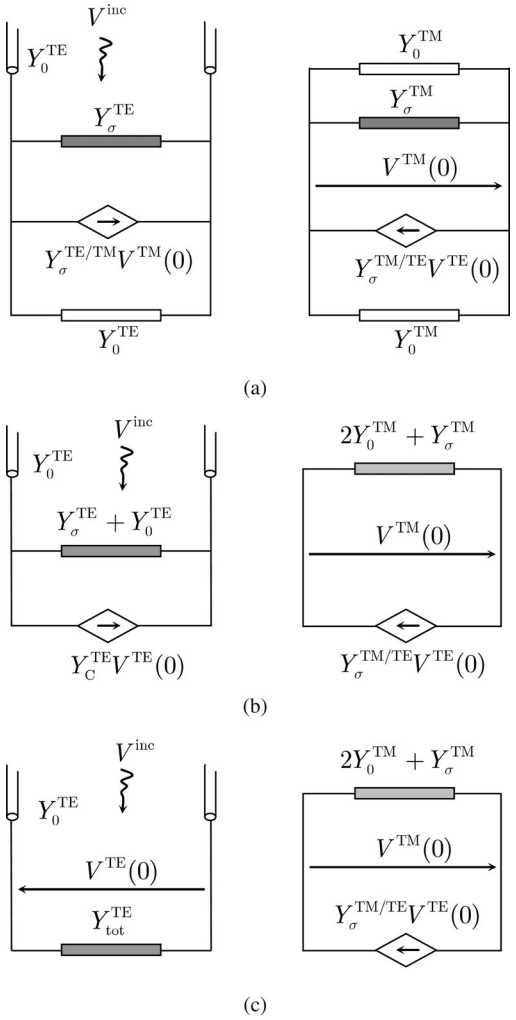

Fig. 4. Equivalent circuits for the TE plane-wave incidence problem.

Now, by observing that the dependent current generator at port 2 is controlled by the voltage at its own terminals, such a generator can simply be substituted by an admittance equal to the controlling parameter $Y_{\rm C}^{\rm TE}$ and the final equivalent circuit is thus reported in Fig. 4(c), where

$$Y_{\rm tot}^{\rm TE}=Y_{\rm C}^{\rm TE}+Y_0^{\rm TE}+Y_\sigma^{\rm TE}=Y_0^{\rm TE}+\sigma_{\rm D}+\frac{\sigma_{\rm O}^2}{2Y_0^{\rm TM}+\sigma_{\rm D}}. \tag{30}$$

The circuit in Fig. 4(c) can now be used to calculate the sought voltages and currents. For instance, it immediately follows that

$$V^{\rm TE}(0)=\left(1+\Gamma^{\rm TE}\right)V^{\rm inc}=\left(1+\frac{Y_0^{\rm TE}-Y_{\rm tot}^{\rm TE}}{Y_0^{\rm TE}+Y_{\rm tot}^{\rm TE}}\right)V_0^{\rm inc}$$
$$=\frac{2Y_0^{\rm TE}}{Y_0^{\rm TE}+Y_{\rm tot}^{\rm TE}}\,V_0^{\rm inc}. \tag{31}$$

From (28) and (31), the derivation of all the other electrical quantities is trivial since

$$I^{\rm TE/TM}\left(0^-\right)=V^{\rm TE/TM}(0)Y_0^{\rm TE/TM}. \tag{32}$$

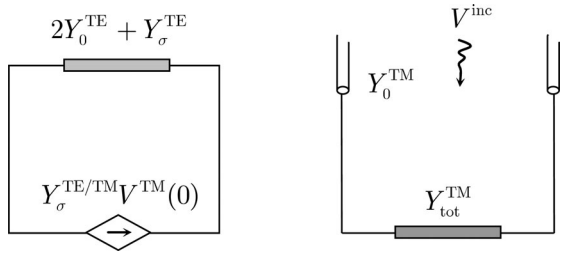

Fig. 5. Equivalent circuit for the TM plane-wave incidence problem.

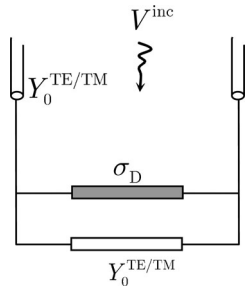

Fig. 6. Equivalent circuit of an isotropic graphene sheet for the TE and TM plane-wave incidence problem.

B. TM Plane-Wave Incidence

When the incident plane wave is TM polarized, the relevant equivalent circuit can be derived with the same steps used to study the TE plane-wave incidence and its final version is reported in Fig. 5. It thus results

$$V^{\rm TE}(0)=\frac{Y_\sigma^{\rm TE/TM}}{2Y_0^{\rm TE}+Y_\sigma^{\rm TE}}\,V^{\rm TM}(0)=\frac{\sigma_{\rm O}}{2Y_0^{\rm TE}+\sigma_{\rm D}}\,V^{\rm TM}(0) \tag{33}$$

and

$$V^{\rm TM}(0)=\frac{2Y_0^{\rm TM}}{Y_0^{\rm TM}+Y_{\rm tot}^{\rm TM}}\,V_0^{\rm inc}, \tag{34}$$

where

$$Y_{\rm tot}^{\rm TM}=Y_{\rm C}^{\rm TM}+Y_0^{\rm TM}+Y_\sigma^{\rm TM}=Y_{\rm C}^{\rm TM}+Y_0^{\rm TM}+\sigma_{\rm D} \tag{35}$$

and

$$Y_{\rm C}^{\rm TM}=-\frac{Y_\sigma^{\rm TE/TM}Y_\sigma^{\rm TM/TE}}{2Y_0^{\rm TE}+Y_\sigma^{\rm TE}}=\frac{\sigma_{\rm O}^2}{2Y_0^{\rm TE}+\sigma_{\rm D}}. \tag{36}$$

Finally, it should be noted that in the absence of a magnetostatic bias and when spatial-dispersion effects can be neglected, the equivalent circuit of the graphene sheet for TE and TM waves is exactly the same and it consists of a simple shunt susceptance $Y_\sigma=\sigma_{\rm D}$, as reported in Fig. 6. From (23), it can be shown that, for $B_{\rm bias}=0$, $\sigma_{\rm DR}>0$ and $\sigma_{\rm DJ}>0$; this means that, in the absence of magnetostatic bias, the graphene sheet can be represented through a series connection of a frequency-dependent resistor and inductor. On the other hand, in the absence of electrostatic bias, while it always results $\sigma_{\rm DR}>0$, the sign of $\sigma_{\rm DJ}$ depends on the value of the applied magnetic field.

C. Shielding Properties

A fundamental parameter for the evaluation of the shielding properties of a planar screen is the shielding effectiveness SE defined as

$$\mathrm{SE}(\mathbf{r}) = -20\log T(\mathbf{r}) \tag{37}$$

where the transmission coefficient T is

$$T(\mathbf{r}) = \frac{|\,\mathbf{E}(\mathbf{r})|}{|\,\mathbf{E}^{\mathrm{inc}}(\mathbf{r})|} \tag{38}$$

while $\mathbf{E}^{\mathrm{inc}}$ is the incident field (in the absence of the graphene sheet) and $\mathbf{r}$ is the observation point in the halfspace $z<0$; however, because of the plane-wave propagation, T (and thus SE) does not depend on the observation point $\mathbf{r}$. For a TE and a TM incident plane wave, from (2) and (6) (with (32) and (3)) we have

$$\mathbf{E}^{\mathrm{inc}}_{\mathrm{TE}}(\mathbf{r}) = \mathbf{e}^{\mathrm{TE}} T(x,y) V_0^{\mathrm{inc}} e^{jk_z z}$$

$$\mathbf{E}^{\mathrm{inc}}_{\mathrm{TM}}(\mathbf{r}) = \left[\mathbf{e}^{\mathrm{TM}} + \sqrt{n_x^2+n_y^2}\,\mathbf{u}_z\right] T(x,y) V_0^{\mathrm{inc}} e^{jk_z z}. \tag{39}$$

In the case of TE incidence, from (27), (28), (31), and (32) it results

$$\begin{aligned}\mathbf{E}(\mathbf{r}) &= T(x,y) V_0^{\mathrm{inc}} e^{jk_z z} \\ &\cdot \left[\mathbf{e}^{\mathrm{TE}} + \left(\mathbf{e}^{\mathrm{TM}} + \sqrt{n_x^2+n_y^2}\,\mathbf{u}_z\right) \frac{\sigma_{\mathrm{O}}}{2Y_0^{\mathrm{TM}}+\sigma_{\mathrm{D}}}\right] \frac{2Y_0^{\mathrm{TE}}}{Y_0^{\mathrm{TE}}+Y_{\mathrm{tot}}^{\mathrm{TE}}} \\ &= \mathbf{e}^{\mathrm{TE}} E^{\mathrm{TE}} + \left(\mathbf{e}^{\mathrm{TM}} + \sqrt{n_x^2+n_y^2}\,\mathbf{u}_z\right) E^{\mathrm{TM}}.\end{aligned} \tag{40}$$

From (38), the first of (39), (40), and because of the ortonormality of the modal vectors, it results

$$T^{\mathrm{TE}}(\theta) = \left|\frac{2Y_0^{\mathrm{TE}}}{Y_0^{\mathrm{TE}}+Y_{\mathrm{tot}}^{\mathrm{TE}}}\right| \sqrt{1+\left|\frac{\sigma_{\mathrm{O}}}{2Y_0^{\mathrm{TM}}+\sigma_{\mathrm{D}}}\right|^2}. \tag{41}$$

The dependence on the incidence angle θ is implicit in the definition of the characteristic admittances Y_0^{TE} and Y_0^{TM}.

For normal incidence (i.e., $\theta=0$), it results $Y_0^{\mathrm{TE}} = Y_0^{\mathrm{TM}} = 1/\eta_0$, and from (30) and (41) we obtain

$$T^{\mathrm{TE}}(0) = \frac{\sqrt{4|2+\sigma_{\mathrm{D}}\eta_0|^2 + |\sigma_{\mathrm{O}}\eta_0|^2}}{|(2+\sigma_{\mathrm{D}}\eta_0)^2 + (\sigma_{\mathrm{O}}\eta_0)^2|}. \tag{42}$$

It should be noted that for an isotropic graphene sheet (not magnetostatically biased and in the absence of spatial dispersion) $\sigma_{\mathrm{O}}=0$ and (42) reduces to

$$T^{\mathrm{TE}}(0) = \frac{2}{|\,2+\sigma_{\mathrm{D}}\eta_0|} \tag{43}$$

which is exactly the same result obtained in [7]. The result in (43) can also immediately be obtained from the equivalent circuit in Fig. 6.

Finally, with similar steps, in the case of TM incidence we obtain

$$T^{\mathrm{TM}}(\theta) = \left|\frac{2Y_0^{\mathrm{TM}}}{Y_0^{\mathrm{TM}}+Y_{\mathrm{tot}}^{\mathrm{TM}}}\right| \sqrt{1+\left|\frac{\sigma_{\mathrm{O}}}{2Y_0^{\mathrm{TE}}+\sigma_{\mathrm{D}}}\right|^2} \tag{44}$$

which for normal incidence and for an isotropic conductivity reduces to (42) and (43), respectively.

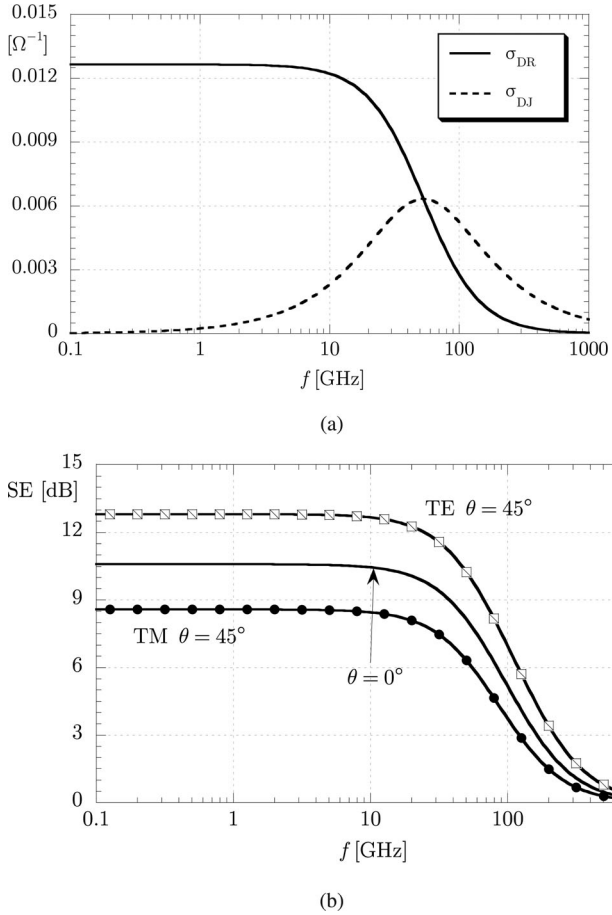

Fig. 7. Graphene conductivity $\sigma_{\mathrm{D}} = \sigma_{\mathrm{DR}} - j\sigma_{\mathrm{DJ}}$ (a) and SE (b) as a function of frequency in the absence of bias fields. Parameters: $T = 300$ K and $\Gamma = 0.11$ meV.

V. Numerical Results

In this section, the electromagnetic behavior of graphene sheets is investigated under different conditions (unbiased, electrostatically biased, and/or magnetostatically biased) in the microwave regime. All results will be presented at room temperature ($T = 300$ K) and for $\Gamma = 1/(2\tau_{\mathrm{S}})$ with $\tau_{\mathrm{S}} = 3$ ns (the same value considered in [9], which corresponds to the electron-acoustic phonon interactions in single-wall carbon nanotubes and which is assumed to be energy- and frequency-independent).

The variation of the graphene conductivity $\sigma_{\mathrm{D}} = \sigma_{\mathrm{DR}} - j\sigma_{\mathrm{DJ}}$ with frequency in the absence of any bias field is reported in Fig. 7(a), where it can be seen that significant changes of the conductivity arise for frequencies larger than 10 GHz up to the THz regime. The behavior of the complex conductivity as a function of frequency simply follows the Drude model in (25); such a behavior reflects the conventional dispersive conductivity arising from a Drude theory of metals, valid provided that spatial-dispersion effects can be neglected, as for the frequency range considered in the present work. For higher frequencies, the dispersive conductivity can be obtained through more sophisticated semiclassical approaches based, e.g., on the Boltzmann transport equation [9].

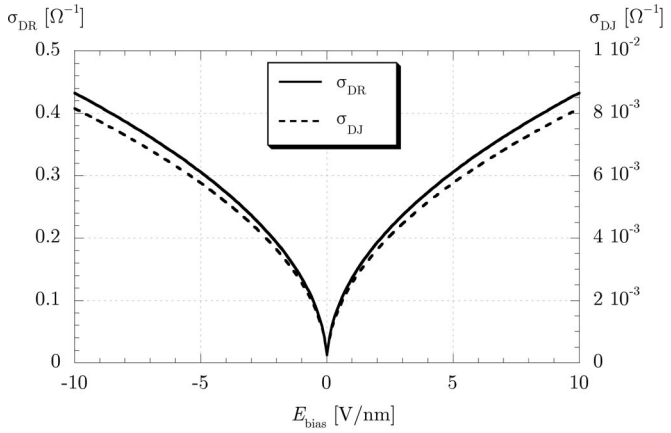

(a)

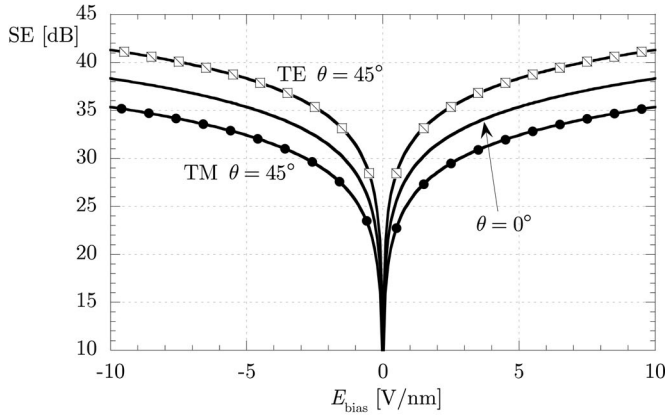

(b)

Fig. 8. Graphene conductivity $\sigma_{\rm D} = \sigma_{\rm DR} - j\sigma_{\rm DJ}$ (a) and SE (b) as a function of the applied electrostatic bias $E_{\rm bias}$ in the absence of magnetostatic fields. Parameters: $T = 300$ K, $\Gamma = 0.11$ meV, and $f = 1$ GHz.

The relevant SE is reported in Fig. 7(b) for different polarizations and incident angles; moderate values of SE are obtained in the microwave regime which can also significantly be improved by means of an applied electrostatic bias $E_{\rm bias}$. In fact, in Fig. 8(a), the variation of $\sigma_{\rm D}$ against $E_{\rm bias}$ is reported at the operating frequency $f = 1$ GHz and in the absence of magnetostatic fields, while in Fig. 8(b) the relevant SE is shown. As it can be seen, the isotropic conductivity is an even function of $E_{\rm bias}$ while better shielding performances are obtained for both polarizations by applying an electrostatic bias.

Considering that graphene is basically a one-atom-thick material, the relevant shielding performances are rather good. This can also be appreciated by observing Fig. 9, where the SE is reported as a function of frequency for graphene sheets with $E_{\rm bias} = 0$ V/nm and $E_{\rm bias} = 5$ V/nm, respectively, and two different thin metal films with typical shielding materials, i.e., a copper casting alloy film with $\mu_{\rm r} = 1$ and $\sigma = 11.8 \cdot 10^6$ S/m and a Duranickel film with $\mu_{\rm r} = 10.58$ and $\sigma = 2.3 \cdot 10^6$ S/m: for simplicity, the conductivities are assumed to be frequency-independent. The thickness t of the metals is chosen equal to $t = 1\mu$m and $t = 10$ nm; such values are of course not practical,

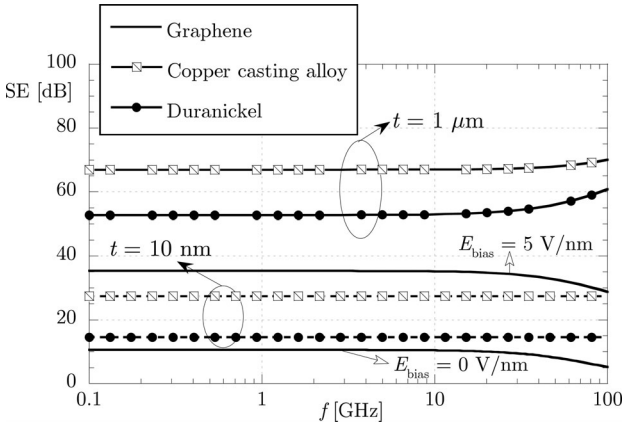

Fig. 9. SE as a function of frequency for unbiased and electrostatically-biased graphene and micro- or nano-thick metal films. Parameters of graphene are as in Fig. 7.

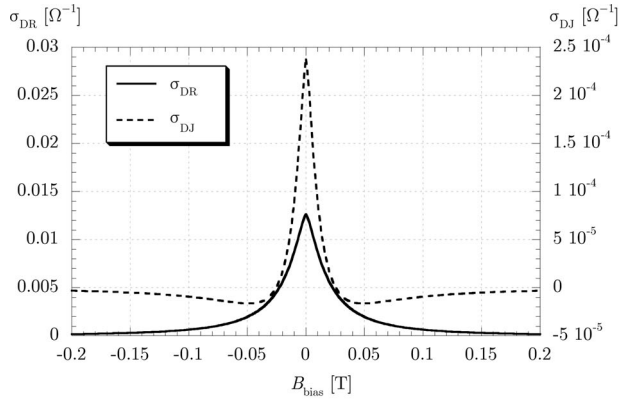

(a)

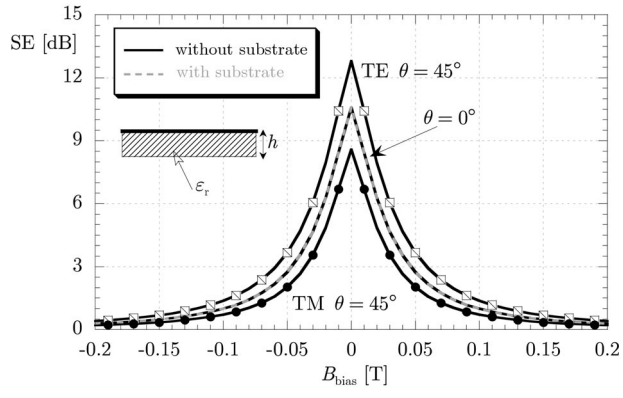

(b)

Fig. 10. Graphene conductivity $\sigma_{\rm D} = \sigma_{\rm DR} - j\sigma_{\rm DJ}$ (a) and SE (b) as a function of the applied magnetostatic bias $B_{\rm bias}$ in the absence of electrostatic fields. Parameters as in Fig. 8.

but they are used only to point out the good shielding performance of graphene despite its infinitesimal thickness, as can be observed in Fig. 9, especially in the electrostatically biased case.

It is also interesting to investigate the effects of a magnetostatic bias field; in the absence of an electrostatic bias, the relevant conductivity and SE results are reported in Fig. 10(a)

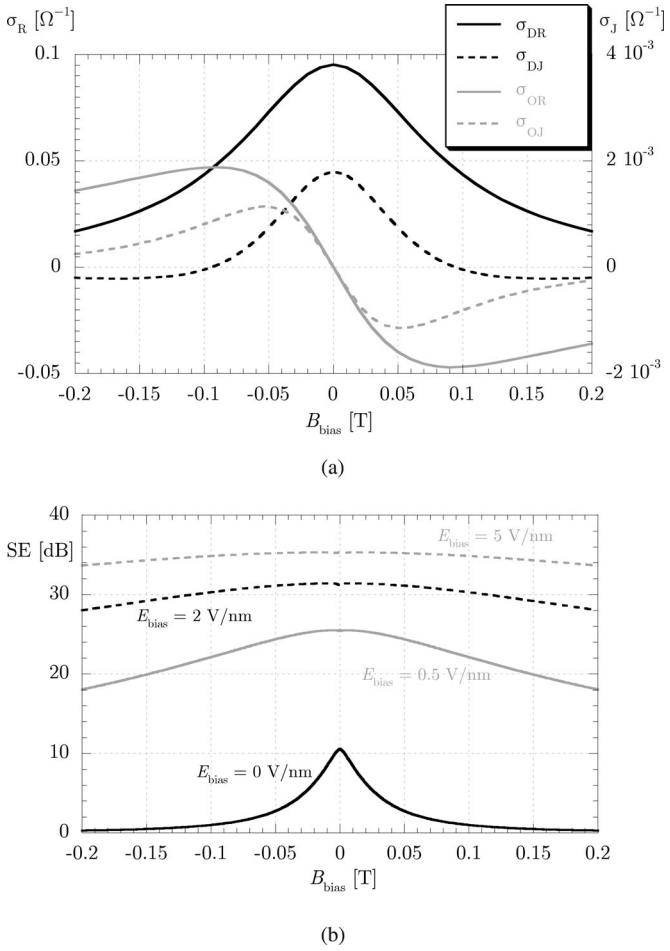

Fig. 11. Diagonal and off-diagonal components of the graphene conductivity tensor (a) and SE (b) as a function of the applied magnetostatic bias $B_{\rm bias}$ for different values of the electrostatic bias field and for normal incidence. Parameters as in Fig. 8.

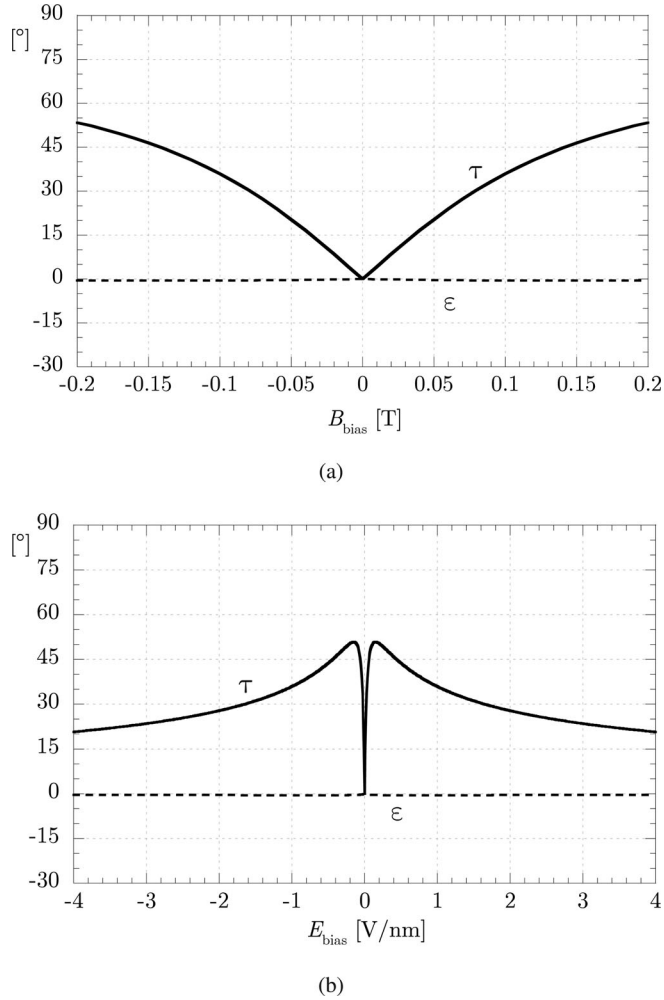

Fig. 12. Angles ε and τ describing the polarization state of the transmitted wave as functions of the magnetostatic bias $B_{\rm bias}$ for $E_{\rm bias} = 1$ V/nm (a) and as functions of the electrostatic bias $E_{\rm bias}$ for $B_{\rm bias} = 0.1$ T (b). Other parameters: $\theta = 0^\circ$ and $f = 1$ GHz.

and (b), respectively, at the frequency $f = 1$ GHz. It can clearly be seen that the applied magnetostatic bias dramatically decreases the conductivity (because of the Hall effect) and makes transparent the graphene sheet. Moreover, the presence of a nanometric board (whose presence can easily be incorporated in the equivalent circuit through a finite length of transmission line) does not influence the shielding performance; in particular, a SiO_2 substrate with thickness $h = 5$ μm and $\varepsilon_{\rm r} \simeq 3.9$ as in the inset of Fig. 10(b) has been considered for normal incidence and the relevant curve is reported in a dashed gray line.

As described in the previous sections, the application of both an electrostatic *and* a magnetostatic bias makes the graphene an anisotropic conductivity surface and several interesting effects can be obtained. In Fig. 11(a), the components of the conductivity tensor $\sigma_{\rm D} = \sigma_{\rm DR} - j\sigma_{\rm DJ}$ and $\sigma_{\rm O} = \sigma_{\rm OR} - j\sigma_{\rm OJ}$ are reported as functions of the applied magnetostatic bias in the presence of an electrostatic bias $E_{\rm bias} = 0.5$ V/nm, again at the operating frequency $f = 1$ GHz: contrarily to the previous isotropic cases, now, for sufficiently large $B_{\rm bias}$, it results $\sigma_{\rm DJ} < 0$ and the diagonal and off-diagonal components are even and odd functions of the applied $B_{\rm bias}$, respectively. In Fig. 11(b), the SE is reported as a function of the applied magnetostatic bias $B_{\rm bias}$ for different values of the electrostatic bias field and for normal incidence at $f = 1$ GHz: it can be seen that, compared to the purely magnetostatically biased case, the presence of an electric field greatly reduces the dependence of the shielding properties on the magnetic-field amplitude.

Another interesting property of graphene in its magnetostatically and electrostatically biased state concerns the possibility of coupling TE and TM waves: If a TE plane wave impinges on the graphene sheet, the transmitted field will consist of both a TE and a TM wave. In order to quantify the degree of polarization rotation, the classical parameters ε and τ adopted to localize the polarization state of a uniform plane wave on the Poincaré sphere are used [16] (in the considered cases, the tilt angle τ represents the tilt of the polarization ellipse with respect to an axis parallel to $\mathbf{e}^{\rm TE}$). Such parameters are reported in Fig. 12(a) and (b) as functions of the magnetostatic bias $B_{\rm bias}$ for $E_{\rm bias} = 1$ V/nm and as functions of the electrostatic bias $E_{\rm bias}$ for $B_{\rm bias} = 0.1$ T, respectively; in both cases, a normal incidence ($\theta = 0^\circ$) at the operating frequency $f = 1$ GHz is

considered. It can be seen that both τ and ε are even functions of both $B_{\rm bias}$ and $E_{\rm bias}$; moreover, it practically results $\varepsilon \simeq 0^\circ$ for all the considered values of the bias fields. This entails that the transmitted wave is always linearly polarized, but thanks to the TE/TM coupling properties, the tilt angle can be tuned over a very wide range of values by the application of a bias field; such properties thus suggest the use of graphene layers also as polarization rotators.

VI. Conclusion

An equivalent circuit is proposed for a simple analysis of the transmitting properties of graphene sheets against electromagnetic plane waves. The equivalent circuit takes into account the anisotropic behavior of the graphene conductivity (which arises because of possible electrostatic and magnetostatic bias or spatial-dispersion effects) and the consequent coupling between fundamental TE and TM polarizations. The electrostatic and/or magnetostatic bias can be used to tune the graphene conductivity which thus entails an electronic control of the relevant shielding properties and the possible use of biased graphene as polarization rotator. Numerical results are provided which illustrate this interesting behavior and its potential applications in electromagnetic shielding.

References

[1] A. K. Geim and K. S. Novoselov, "The rise of graphene," *Nature Mater.*, vol. 6, pp. 183–191, Mar. 2007.

[2] A. K. Geim, "Graphene: Status and prospects," *Science*, vol. 324, pp. 1530–1532, 2009.

[3] K. S. Novoselov, A. K. Geim, S. V. Morozov, D. Jiang, Y. Zhang, S. V. Dubonos, I. V. Grigorieva, and A. A. Firsov, "Electric field effect in atomically thin carbon films," *Science*, vol. 306, pp. 666–669, 2004.

[4] Y. Zhang, Y.-W. Tan, H. L. Stormer, and P. Kim, "Experimental observation of the quantum Hall effect and Berry's phase in graphene," *Nature*, vol. 438, pp. 201–204, 2005.

[5] K. S. Novoselov, A. K. Geim, S. V. Morozov, D. Jiang, M. I. Katnelson, I. V. Grigorieva, S. V. Dubonos, and A. A. Firsov, "Two-dimensional gas of massless Dirac fermions in graphene," *Nature*, vol. 438, pp. 197–200, 2005.

[6] A. H. Castro Neto, F. Guinea, N. M. R. Peres, K. S. Novoselov, and A. K. Geim, "The electronic properties of graphene," *Rev. Mod. Phys.*, vol. 81, no. 1, pp. 109–162, Jan. 2009.

[7] G. W. Hanson, "Dyadic Green's function and guided surface waves for a surface conductivity model of graphene," *J. Appl. Phys.*, vol. 103, p. 064302, 2008.

[8] V. P. Gusynin, S. G. Sharapov, and J. P. Carbotte, "Magneto-optical conductivity in graphene," *J. Phys.: Cond. Matter*, vol. 19, no. 2, p. 026222, 2007.

[9] G. W. Hanson, "Dyadic Green's functions for an anisotropic non-local model of biased graphene," *IEEE Trans. Antennas Propag.*, vol. 56, no. 3, pp. 747–757, Mar. 2008.

[10] S. Celozzi, R. Araneo, and G. Lovat, *Electromagnetic Shielding*. Hoboken, NJ: Wiley-IEEE, 2008.

[11] M. Sarto, F. Sarto, M. Larciprete, M. Scalora, M. D'Amore, C. Sibilia, and M. Bertolotti, "Nanotechnology of transparent metals for radio frequency electromagnetic shielding," *IEEE Trans. Electromagn. Compat.*, vol. 45, no. 4, pp. 586–594, Nov. 2003.

[12] I. De Rosa, R. Mancinelli, F. Sarasini, M. Sarto, and A. Tamburrano, "Electromagnetic design and realization of innovative fiber-reinforced broadband absorbing screens," *IEEE Trans. Electromagn. Compat.*, vol. 51, no. 3, pp. 700–707, Aug. 2009.

[13] G. Antonini, A. Orlandi, and L. Raimondo, "Advanced models for signal integrity and electromagnetic compatibility-oriented analysis of nanointerconnects," *IEEE Trans. Electromagn. Compat.*, vol. 52, no. 2, pp. 447–454, May 2010.

[14] K. A. Michalski and J. R. Mosig, "Multilayered media Green's functions in integral equation formulations," *IEEE Trans. Antennas Propag.*, vol. 45, no. 3, pp. 508–519, Mar. 1997.

[15] M. Dressel and G. Grüner, *Electrodynamics of Solids*. Cambridge, UK: Cambridge Univ. Press, 2002.

[16] C. A. Balanis, *Advanced Engineering Electromagnetics*. New York: Wiley, 1989.

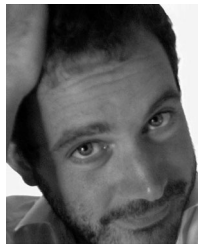

Giampiero Lovat (S'02-M'06) was born in Rome, Italy, on May 31, 1975. He received the Laurea degree (*cum laude*) in electronic engineering and the Ph.D. degree in applied electromagnetics, both from "La Sapienza" University of Rome, Rome, Italy, in 2001 and 2005, respectively.

In 2005, he joined the Electrical Engineering Department of "La Sapienza" University of Rome, Italy, where he is currently an Assistant Professor in the Astronautical, Electrical, and Energetic Engineering Department. From January 2004 to July 2004 he was a Visiting Scholar at the University of Houston, Houston, Texas. He has coauthored the book *Electromagnetic Shielding* (Hoboken, NJ: IEEE Wiley, 2008), and the "Fast Breaking Papers, October 2007" in EE and CS, about metamaterials (paper that had the highest percentage increase in citations in Essential Science Indicators, ESI). His present research interests include leaky waves, general theory and numerical methods for the analysis of periodic structures, and electromagnetic shielding.

Dr. Lovat received a Young Scientist Award from the 2005 URSI General Assembly, New Delhi, India, and in 2011 he was the recipient of the Best Paper Symposium Award at the 2011 IEEE EMC-S International Symposium on Electromagnetic Compatibility.